

On the wind turbine blade loads from an aeroelastic simulation and their transfer to a three-dimensional finite element model of the blade

Louis-Charles Forcier¹ and Simon Joncas¹

Abstract

This paper first presents a description of the different load types to which a wind turbine blade is subjected. Analytical equations are derived to express blade loads from operation parameters of the wind turbine (rotor and nacelle velocities and accelerations; pitch, coning, tilt and azimuth angles; blade mass properties; turbine geometry). This allows a better understanding of the contribution of each of these parameters to the total load on a blade. A difficulty arises for transferring the loads computed by an aeroelastic model (a one-dimensional model of the blade) to a three-dimensional finite element model of the blade. A method is proposed for that purpose. It consists in applying the aerodynamic loads using RBE3 elements and applying gravitational and inertial loads as volume forces. Finally, an example of this method used for the design of a 10 kW wind turbine blade is presented.

Keywords

Wind turbine blade, finite element model, load application, wind turbine blade loads

Introduction

Aeroelastic simulations are frequently used for the design and analysis of wind turbines. Tools like FAST (Jonkman and Buhl Jr. 2005), GH Bladed (Bossanyi 2003), HAWC2 (Larsen and Hansen 2007) or

¹ Department of Systems Engineering, École de technologie supérieure, Montréal, Canada

Corresponding author:

Louis-Charles Forcier, Department of Systems Engineering, École de technologie supérieure, 1100 Notre-Dame West Street, Montréal, H3C 1K3, Canada
Email: louis-charles.forcier.1@ens.etsmtl.ca

PHATAS, a module of FOCUS6 (Knowledge Centre WMC 2012; Lindenburg 2005), allow the simulation of the fully coupled dynamic behavior of the wind turbine. Three methods are mostly used to model the structural behavior of the deformable blades: multibody dynamics (a series of rigid bodies linked with springs); beam finite element; and modal superposition (the blade deflection is a weighted sum of its first modal shapes).

The Elastodyn module of FAST uses modal superposition with the first two flapwise and the first edgewise modes. The blade deformation is then given by 3 parameters (generalized coordinates that are scaling factors for each mode shape). Torsion is not taken into account. GH Bladed also uses this method with up to 6 modes in each blade directions. Like FAST (using the Elastodyn module), no torsional degrees of freedom are modeled. Both software work under the small perturbation assumption for the blade deformation. However, in FAST, the loads are computed on the deformed shape of the blade, allowing the modeling of some nonlinear effects (Jonkman 2003; Wilson et al. 1999).

HAWC2 uses a combination of beam finite elements and multibody dynamics. Blades can be modeled with several bodies made of Timoshenko beam finite elements allowing the modeling of all the couplings between the different modes of deformation. This method also takes into account the nonlinear behavior of the blade even if linear models are used for the beam elements. When using the Beamdyn module of FAST, the blades are modeled using geometric nonlinear beam finite elements. These elements use a Timoshenko beam formulation and have capabilities to model all possible couplings between the different modes of deformation (Wang et al. 2017).

All these methods are based on beam theory and need to evaluate the different cross section properties along the blade length. Tools for that purpose include PreComp (Bir 2005), VABS (Yu et al. 2002), CROSTAB (Lindenburg and de Winkel 2005b), FAROB, a module of FOCUS6 (Lindenburg and de Winkel 2005b) and BECAS (Blasques 2012). These software packages, excluding VABS and BECAS, use Euler-Bernoulli beam theory and shear flow analysis of thin-walled beams to compute axial, bending and torsion section moduli as well as coupling terms between these modes of deformation. VABS and BECAS uses the Timoshenko beam theory so they also include shear deformation due to shear forces. For a review of some of these different software packages, see the article by Chen et al. (2010).

Another tool for blade cross-section properties calculations is BPE (Malcolm and Laird 2007), which use a shell or solid finite element model. A set of unit loads is applied to the blade tip and section properties are computed from the analysis of nodal displacement at different cross-section along the blade length.

Once the internal loads have been computed at different blade sections during the aeroelastic simulation, the section modulus can be used to compute strains and stresses in these cross sections. Unfortunately, this method gives good results only in regions away from the blade attachment and when cross section shape variations are small (Chen et al. 2010), which is not the case at the blade root and near the maximum chord region. It is also possible to evaluate the buckling load of a cross-section or of a panel in a cross-section, but these methods are less accurate than with three-dimensional finite element models (Lindenburg and de Winkel 2005a).

Three dimensional finite element models (using shell or solid elements) can give a more precise strain and stress field on the blade but these models can be included in aeroelastic simulations only at a very prohibitive computational cost. For an example of aeroelastic simulation using shell model of the blade and computation fluid dynamics, see the articles by Bazilevs et al. (2011a,b).

A trade-off between efficient aeroelastic simulations and high precision strain, stress and buckling evaluation of the blade is to use the aeroelastic simulation to identify the critical load cases and reproduce them on a three-dimensional finite element model. However, the transfer from one dimensional beam load to three-dimensional models is not straightforward.

If the load case to analyze is when the blade is at rest or if the gravitational and inertial forces are negligible, only aerodynamic loads have to be applied to the model. A way of doing that is to apply a concentrated force at the nearest node from each blade element center corresponding to the aerodynamic force at this blade element (see for example a report by Griffith and Ashwill (2011)). Another way is to try to reproduce the pressure field on the blade surface using the blade airfoil properties and the angles of attack computed by the aerodynamic analysis tool (see for example the work of Knill (2005) and Caous et al. (2018)).

If gravitational loads have to be considered in the analysis, it is easy to apply them as volume loads in the finite element model. One just has to compute the gravity vector direction according to the blade orientation in space.

Inertial loads on the blade can be calculated from the blade acceleration relative to an inertial coordinate system and from the blade mass distribution (see for example the work of Lillo (2011)).

Another approach is to use the total load computed by the aeroelastic solver (including aerodynamic, gravitational and inertial) as internal loads given at specific locations along the blade length. The external load distribution that generates this internal load distribution can then be computed and applied to the shell finite element model as point or distributed loads as discussed in the section beginning at page 14.

The proposed approach of this paper is to use the operation parameters of the wind turbine (rotor and nacelle rotational speed and acceleration, blade azimuth, blade pitch, rotor coning and rotor tilt) to characterize the inertial loads on the blade. This facilitates the inclusion of these loads in a finite element model as volume loads. In doing so, the mass distribution of the blade around its longitudinal axis is taken into account and a change in the design that affects the blade mass distribution is also taken into account in the applied loads.

The objectives of this paper are twofold. First, it is to derive analytical expressions for the gravitational and inertial load distribution on a wind turbine blade from the blade mass distribution and the turbine operation parameters. This will allow (1) the separation of the total load obtained from aeroelastic simulation in its different types and; (2) the understanding of the influence of different wind turbine operating parameters on blade loads. The second objective is to develop a tool to reproduce the loads from an aeroelastic simulation on a three-dimensional finite element model of the wind turbine blade by separating the different load types.

The next section will discuss the different types of loads on a wind turbine blade and the approach used to evaluate them. An expression for the distribution of each type of load on the blade will then be presented with the resulting forces and moments at the blades root. Next, a methodology will be presented to apply all these loads on a three-dimensional finite element model of a wind turbine blade, and finally, an example of this methodology will be applied on a 10 kW wind turbine.

Loads on a wind turbine blade and methodology

For a given particle P of mass m on the blade, the Newton's second law can be written as

$$\mathbf{F}_{aero} + \mathbf{F}_{grav} + \mathbf{R} = m\mathbf{a}_{P/G} \quad (1)$$

where \mathbf{F}_{aero} , \mathbf{F}_{grav} and $\mathbf{a}_{P/G}$ are respectively the aerodynamic force vector, the gravitational force vector and the acceleration of point P relative to an inertial coordinate system. Vector \mathbf{R} is the reaction force due to the blade deformation. Note that the damping forces are neglected.

If we want to perform a static analysis of the blade, we can rewrite the Newton's second law as

$$\mathbf{F}_{aero} + \mathbf{F}_{grav} + \mathbf{F}_{iner} + \mathbf{R} = 0 \quad (2)$$

where the inertial loads are

$$\mathbf{F}_{iner} = -m\mathbf{a}_{P/G} \quad (3)$$

It is then possible to apply aerodynamic, gravitational and inertial loads on a static model of the blade to evaluate the displacement, strain and stress fields for a dynamic load case.

The wind turbine model that allows the computation of the different loads has seven coordinate systems as shown in Figure 1. The origin of the *blade coordinate system* (\cdot_b) is located at blade root and is fixed to the blade (pitches with the blade). The z axis is parallel to the blade's longitudinal axis (and pointing towards blade tip) and the x axis is parallel to the blade tip chord line (and pointing towards leading edge). A positive pitch θ (leading edge goes upwind) is a rotation of the blade around its negative z axis. In the finite element model of the blade presented later, the global coordinate system is the blade coordinate system.

The *cone coordinate system* (\cdot_c) is identical to the blade coordinate system but does not pitch with the blade. It is aligned with the blade coordinate system when $\theta = 0$.

The origin of the *hub coordinate system* (\cdot_h) is located at the intersection of the rotor axis of rotation and the blade longitudinal axis. It rotates with the rotor. The z axis is parallel to the blade's longitudinal axis projection in the rotor plane and the y axis is normal to the rotor plane. The rotor turns clockwise (around positive y axis) when looking from upwind.

The *tilt coordinate system* (\cdot_t) is fixed to the nacelle and tilted. It is the same as the hub coordinate system when the azimuth angle $\Psi = 0$ (blade pointing upward).

The *nacelle coordinate system* (\cdot_n) is fixed to the nacelle, but not tilted. The z axis is pointing upward and the y axis is normal to the rotor plane (if $\gamma = 0$) and is pointing downwind (assuming no yaw error). The origin of this coordinate system passes through the tower axis.

The *tower top coordinate system* (\cdot_T) is fixed to the tower top. It is the same as the nacelle coordinate system when the yaw angle is zero.

Finally, the *ground coordinate system* (\cdot_G) is an inertial coordinate system. Its origin is located at the intersection of the tower's longitudinal axis and the ground level. The x and y axis of this coordinate system are aligned to the x and y axis of the tower top coordinate system respectively.

Here, all wind turbine components, except for the tower and the blades, are considered to be rigid. If $\mathbf{r}_{j/i}$, $\mathbf{v}_{j/i}$, $\mathbf{a}_{j/i}$, $\boldsymbol{\omega}_{j/i}$ and $\boldsymbol{\alpha}_{j/i}$ are respectively the position, velocity, acceleration, angular velocity and angular acceleration of point j (or origin of coordinate system j) relative to the coordinate system i , we can establish the following relations between coordinate systems: $\boldsymbol{\omega}_{n/T} = [0, 0, \Lambda]_n^T$, $\boldsymbol{\alpha}_{n/T} = [0, 0, \dot{\Lambda}]_n^T$, $\mathbf{r}_{t/n} = [0, -L_{nr}, 0]_t^T$, $\boldsymbol{\omega}_{h/t} = [0, \Omega, 0]_h^T$, $\boldsymbol{\alpha}_{h/t} = [0, \dot{\Omega}, 0]_h^T$, $\mathbf{r}_{c/h} = [0, 0, r_h]_c^T$, $\boldsymbol{\omega}_{b/c} = [0, 0, \dot{\theta}]_b^T$, $\boldsymbol{\alpha}_{b/c} = [0, 0, \ddot{\theta}]_b^T$. The indices after the vectors show in which coordinate system the vector components are expressed. All other position, velocity and acceleration vectors between two adjacent coordinate system in the kinematic chain (blade, cone, hub, tilt, nacelle, tower top, ground coordinate systems) are zero vectors. Λ and $\dot{\Lambda}$ are respectively the nacelle yaw velocity

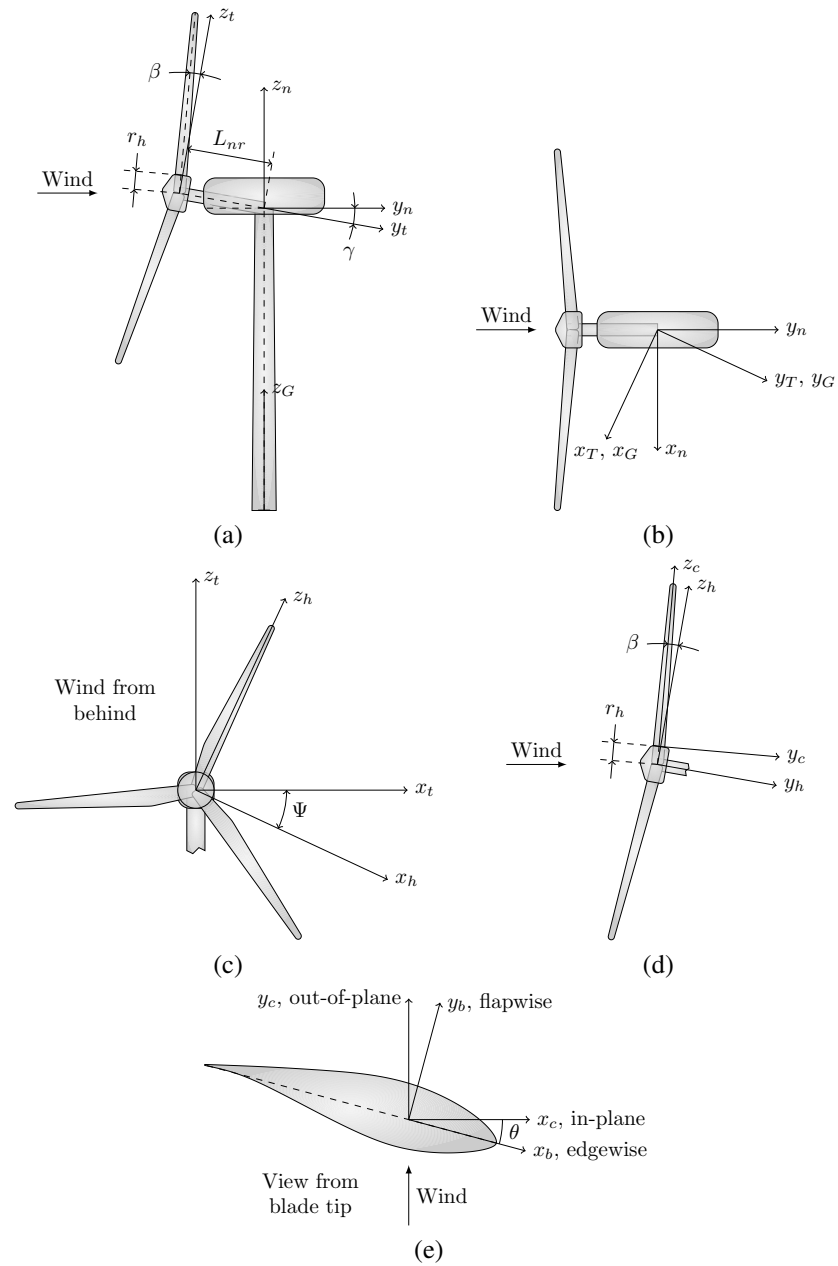


Figure 1. Coordinate systems used in the wind turbine model.

and acceleration, Ω and $\dot{\Omega}$ are respectively the rotor rotational velocity and acceleration, $\dot{\theta}$ and $\ddot{\theta}$ are respectively the blade pitch angular velocity and acceleration, r_h is the hub radius (distance between blade root and the rotor axis parallel to blade axis), L_{nr} is the distance between the origin of the hub coordinate system and the nacelle yaw axis normal to the rotor axis and γ is the rotor tilt angle.

To the relations between coordinate systems stated above, we have to add the tower top motion relative to the ground. Vectors $\boldsymbol{\omega}_{T/G}$, $\boldsymbol{\alpha}_{T/G}$ and $\mathbf{a}_{T/G}$ are not null when the tower is flexible.

The transformation matrices from one coordinate system to another are:

$$\mathbf{P}_{b/c} = \begin{bmatrix} c_\theta & -s_\theta & 0 \\ s_\theta & c_\theta & 0 \\ 0 & 0 & 1 \end{bmatrix} \quad (4)$$

$$\mathbf{P}_{c/h} = \begin{bmatrix} 1 & 0 & 0 \\ 0 & c_\beta & s_\beta \\ 0 & -s_\beta & c_\beta \end{bmatrix} \quad (5)$$

$$\mathbf{P}_{h/t} = \begin{bmatrix} c_\Psi & 0 & -s_\Psi \\ 0 & 1 & 0 \\ s_\Psi & 0 & c_\Psi \end{bmatrix} \quad (6)$$

$$\mathbf{P}_{t/n} = \begin{bmatrix} 1 & 0 & 0 \\ 0 & c_\gamma & -s_\gamma \\ 0 & s_\gamma & c_\gamma \end{bmatrix} \quad (7)$$

where θ , β , Ψ and γ are respectively the pitch, rotor coning, blade azimuth and rotor tilt angles. $c_i = \cos i$ and $s_i = \sin i$.

We know from kinematics that the expressions of acceleration $\mathbf{a}_{P/i}$, velocity $\mathbf{v}_{P/i}$ and position $\mathbf{r}_{P/i}$ of a point P in a coordinate system i when the acceleration $\mathbf{a}_{P/j}$, velocity $\mathbf{v}_{P/j}$ and position $\mathbf{r}_{P/j}$ of this point in coordinate system j are known are:

$$\begin{cases} \mathbf{a}_{P/i} = \mathbf{a}_{P/j} + \mathbf{a}_{j/i} + 2\boldsymbol{\omega}_{j/i} \times \mathbf{v}_{P/j} \\ \quad + \boldsymbol{\omega}_{j/i} \times \boldsymbol{\omega}_{j/i} \times \mathbf{r}_{P/j} + \boldsymbol{\alpha}_{j/i} \times \mathbf{r}_{P/j} \\ \mathbf{v}_{P/i} = \mathbf{v}_{P/j} + \mathbf{v}_{j/i} + \boldsymbol{\omega}_{j/i} \times \mathbf{r}_{P/j} \\ \mathbf{r}_{P/i} = \mathbf{r}_{P/j} + \mathbf{r}_{j/i} \end{cases} \quad (8)$$

where $\boldsymbol{\omega}_{j/i}$ and $\boldsymbol{\alpha}_{j/i}$ are respectively the angular velocity and the angular acceleration vectors of coordinate system j relative to coordinate system i . Using these equations, and the already stated relations between the different coordinate systems, from Eq. 3, the inertial force on a mass element P on the blade

can be expressed as:

$$\begin{aligned}
 \mathbf{F}_{iner} = & -m\boldsymbol{\omega}_{h/t} \times \boldsymbol{\omega}_{h/t} \times \mathbf{r}_{P/h} && (1- centrifugal, rotor rotation) \\
 & -m\boldsymbol{\alpha}_{h/t} \times \mathbf{r}_{P/h} && (2- inertial, rotor acceleration) \\
 & -m\boldsymbol{\omega}_{n/T} \times \boldsymbol{\omega}_{n/T} \times \mathbf{r}_{P/n} && (3- centrifugal, nacelle rotation) \\
 & -m\boldsymbol{\alpha}_{n/T} \times \mathbf{r}_{P/n} && (4- inertial, nacelle acceleration) \\
 & -2m\boldsymbol{\omega}_{n/T} \times \boldsymbol{\omega}_{h/t} \times \mathbf{r}_{P/h} && (5- gyrosc., rotor and nacelle rot.) \\
 & -m\boldsymbol{\omega}_{b/c} \times \boldsymbol{\omega}_{b/c} \times \mathbf{r}_{P/b} && (6- centrifugal, blade pitch rotation) \\
 & -m\boldsymbol{\alpha}_{b/c} \times \mathbf{r}_{P/b} && (7- inertial, blade pitch acceleration) \\
 & -2m\boldsymbol{\omega}_{h/t} \times \boldsymbol{\omega}_{b/c} \times \mathbf{r}_{P/b} && (8- gyrosc., blade pitching and rotor rot.) \\
 & -2m\boldsymbol{\omega}_{n/T} \times \boldsymbol{\omega}_{b/c} \times \mathbf{r}_{P/b} && (9- gyrosc., blade pitching and nacelle rot.) \\
 & -m\mathbf{a}_{T/G} && (10- tower top motion) \\
 & -2m\boldsymbol{\omega}_{T/G} \times \mathbf{v}_{P/b} && (11- tower top motion) \\
 & -2m\boldsymbol{\omega}_{T/G} \times \boldsymbol{\omega}_{b/c} \times \mathbf{r}_{P/b} && (12- tower top motion) \\
 & -2m\boldsymbol{\omega}_{T/G} \times \boldsymbol{\omega}_{h/t} \times \mathbf{r}_{P/h} && (13- tower top motion) \\
 & -2m\boldsymbol{\omega}_{T/G} \times \boldsymbol{\omega}_{n/T} \times \mathbf{r}_{P/n} && (14- tower top motion) \\
 & -m\boldsymbol{\omega}_{T/G} \times \boldsymbol{\omega}_{T/G} \times \mathbf{r}_{P/T} && (15- tower top motion) \\
 & -m\boldsymbol{\alpha}_{T/G} \times \mathbf{r}_{P/T} && (16- tower top motion) \\
 & -m\mathbf{a}_{P/b} && (17- blade deformation) \\
 & -2m\boldsymbol{\omega}_{b/c} \times \mathbf{v}_{P/b} && (18- blade deformation) \\
 & -2m\boldsymbol{\omega}_{h/t} \times \mathbf{v}_{P/b} && (19- blade deformation) \\
 & -2m\boldsymbol{\omega}_{n/T} \times \mathbf{v}_{P/b} && (20- blade deformation)
 \end{aligned} \tag{9}$$

The first two terms of the equation are the inertial loads due to the rotor rotation. The first one is a centrifugal force and the second one is due to the angular acceleration. The 3rd and 4th terms represent the same effects, but due to the nacelle rotation and angular acceleration. The 5th term is the gyroscopic force due to the combination of rotor and nacelle rotations. Terms 6 to 9 are due to the blade pitch motion and depend on the blade mass distribution around its longitudinal axis. The 7 following terms are the effects of the tower top motion due to the tower deformation and the last 4 terms are due to the blade deformation.

For the development of the next section's equations, two simplifying hypotheses are made. Firstly, we consider that all the blade mass is concentrated on its longitudinal axis, so that terms 6 to 9 vanish. Secondly, the effects of the blade and tower deformation will be neglected. This allows us to more clearly characterize the effects of wind turbine operation parameters on the inertial loads and as the effect that terms 10 to 20 vanish.

With these hypotheses, it is possible to express the inertial load distribution on the blade in terms of force per unit length as:

$$\begin{aligned}
\mathbf{p}_{iner} = & -m' \boldsymbol{\omega}_{h/t} \times \boldsymbol{\omega}_{h/t} \times \mathbf{r}_{P/h} \\
& -m' \boldsymbol{\alpha}_{h/t} \times \mathbf{r}_{P/h} \\
& -m' \boldsymbol{\omega}_{n/T} \times \boldsymbol{\omega}_{n/T} \times \mathbf{r}_{P/n} \\
& -m' \boldsymbol{\alpha}_{n/T} \times \mathbf{r}_{P/n} \\
& -2m' \boldsymbol{\omega}_{n/T} \times \boldsymbol{\omega}_{h/t} \times \mathbf{r}_{P/h}
\end{aligned} \tag{10}$$

where m' is the mass per unit length of the blade. The vectors expressed in the blade coordinate system are :

$$\mathbf{r}_{P/h} = \begin{bmatrix} 0 \\ 0 \\ z + r_h \end{bmatrix} \tag{11}$$

$$\mathbf{r}_{P/n} = \begin{bmatrix} L_{nr} c_\beta s_\theta \\ -L_{nr} c_\beta c_\theta \\ z + r_h + L_{nr} s_\beta \end{bmatrix} \tag{12}$$

$$\boldsymbol{\omega}_{h/T} = \Omega \mathbf{A}_h \tag{13}$$

$$\boldsymbol{\omega}_{n/T} = \Lambda \mathbf{A}_n \tag{14}$$

$$\boldsymbol{\alpha}_{h/T} = \dot{\Omega} \mathbf{A}_h \tag{15}$$

$$\boldsymbol{\alpha}_{n/T} = \dot{\Lambda} \mathbf{A}_n \tag{16}$$

where \mathbf{A}_h and \mathbf{A}_n are unit vectors defined as

$$\mathbf{A}_h = \begin{bmatrix} -c_\beta s_\theta \\ c_\beta c_\theta \\ -s_\beta \end{bmatrix} \tag{17}$$

and

$$\mathbf{A}_n = \begin{bmatrix} -(s_\beta c_\gamma c_\Psi - c_\beta s_\gamma) s_\theta - c_\gamma s_\Psi c_\theta \\ (s_\beta c_\gamma c_\Psi - c_\beta s_\gamma) c_\theta - c_\gamma s_\Psi s_\theta \\ c_\beta c_\gamma c_\Psi + s_\beta s_\gamma \end{bmatrix} \tag{18}$$

Distribution of loads on the blade and blade root loads

In this section, an analytical expression is given for the loads distribution on the blade for each load type. Internal loads at blade root are also given as they are often used to compare load cases with each other. All vector components are expressed in the blade coordinate system.

Load distribution along blade length is defined by $\mathbf{p}(z) = [p_x(z), p_y(z), p_z(z)]^T$ and $\mathbf{m}(z) = [m_x(z), m_y(z), m_z(z)]^T$, which are respectively the applied forces and moments per unit length. The internal loads are $\mathbf{V}(z) = [V_x(z), V_y(z), N(z)]^T$ where $V_x(z)$ and $V_y(z)$ are the shear forces and $N(z)$ is the normal force; and $\mathbf{M}(z) = [M_x(z), M_y(z), M_t(z)]^T$ where $M_x(z)$ and $M_y(z)$ are the bending moments and $M_t(z)$ is the torsional moment.

Aerodynamic loads

Aerodynamic loads are computed by the aerodynamic routine of the aeroelasticity code using mostly blade element momentum theory. Aerodynamic forces along blade length are computed in the in-plane (p_{in}) and out-of-plane directions (p_{out}), respectively parallel to the x and y axis of the coned coordinate system). The radial aerodynamic force is neglected most of the time. The aerodynamic pitching moment m_p (positive when pitch angle is decreased) is also computed by the aerodynamic solver.

In the blade coordinate system, the aerodynamic force and moment distributions are given by

$$\mathbf{p}_{aero}(z) = \begin{bmatrix} p_{in}c\theta - p_{out}s\theta \\ p_{in}s\theta + p_{out}c\theta \\ 0 \end{bmatrix} \quad (19)$$

and

$$\mathbf{m}_{aero}(z) = \begin{bmatrix} 0 \\ 0 \\ m_p \end{bmatrix} \quad (20)$$

where θ is the blade pitch angle.

The integration of these loads along blade length allow the computation of the blade root internal loads as:

$$\mathbf{V}_{aero}(0) = \int_0^L \mathbf{p}_{aero} dz \quad (21)$$

and

$$\mathbf{M}_{aero}(0) = \int_0^L \begin{bmatrix} -zp_{y,aero} \\ zp_{x,aero} \\ m_{z,aero} \end{bmatrix} dz \quad (22)$$

where L is the length of the blade. Note that these last two equations are still valid for any types of loads.

Depending on the aerodynamic code used, these forces can be distributed forces (per unit length of the blade) computed at some location. Internal loads at blade root are then computed by numerical integration of equations 19 and 20 using, for instance, linear interpolation between these locations (Hansen 2008). Other codes (Jonkman and Buhl Jr. 2005) compute concentrated loads at each aerodynamic blade element center. Internal loads at blade root can then computed using a summation instead of an integral in equations 19 and 20.

Gravitational loads

The gravitational force distribution along the blade is given by

$$\mathbf{p}_{grav}(z) = m' \mathbf{g} \quad (23)$$

where \mathbf{g} is the gravitational acceleration vector ($\|\mathbf{g}\| = g \approx 9.81 \text{ m/s}^2$), whose components are $[0, 0, -1]_n^T$ when expressed in the nacelle coordinate system. The force direction then depends on the orientation of the blade in space, i.e., pitch, azimuth, coning and tilt angles.

In the blade coordinate system, the gravitational force distribution is given by:

$$\mathbf{p}_{grav}(z) = m'g \begin{bmatrix} c_\gamma s_\Psi c_\theta - (c_\beta s_\gamma - s_\beta c_\gamma c_\Psi) s_\theta \\ c_\gamma s_\Psi s_\theta + (c_\beta s_\gamma - s_\beta c_\gamma c_\Psi) c_\theta \\ -s_\beta s_\gamma - c_\beta c_\gamma c_\Psi \end{bmatrix} \quad (24)$$

and the internal loads at the blade root are

$$\mathbf{V}_{grav}(0) = mg \begin{bmatrix} c_\gamma s_\Psi c_\theta - (c_\beta s_\gamma - s_\beta c_\gamma c_\Psi) s_\theta \\ c_\gamma s_\Psi s_\theta + (c_\beta s_\gamma - s_\beta c_\gamma c_\Psi) c_\theta \\ -s_\beta s_\gamma - c_\beta c_\gamma c_\Psi \end{bmatrix} \quad (25)$$

and

$$\mathbf{M}_{grav}(0) = Z_{cg}mg \begin{bmatrix} -c_\gamma s_\Psi s_\theta - (c_\beta s_\gamma - s_\beta c_\gamma c_\Psi) c_\theta \\ c_\gamma s_\Psi c_\theta - (c_\beta s_\gamma - s_\beta c_\gamma c_\Psi) s_\theta \\ 0 \end{bmatrix} \quad (26)$$

where m and Z_{cg} are respectively the total blade mass and the distance between the blade root and the blade center of gravity:

$$m = \int_0^L m' dz \quad (27)$$

and

$$Z_{cg} = \frac{1}{m} \int_0^L m' z dz \quad (28)$$

Assuming that the coning and tilt angles are small, which is the case for most horizontal axis wind turbine, and that pitch angle is close to zero, which is the case below nominal wind speed, gravity causes a mostly axial load when the blade is pointing upward and downward and a mostly edgewise load when the blade is in the horizontal position. If the blade is in the feather position (pitch angle close to 90°), in the horizontal position, gravity causes a mostly flapwise loading.

Inertial loads due to rotor rotation

This load type is given by the first term of Eq. 10. When loads are expressed in the blade coordinate system,

$$\mathbf{p}_{iner,1}(z) = m'\Omega^2(z + r_h)c_\beta \begin{bmatrix} -s_\beta s_\theta \\ s_\beta c_\theta \\ c_\beta \end{bmatrix} \quad (29)$$

and the integration over the blade length gives the following expressions for the internal loads at blade root:

$$\mathbf{V}_{iner,1}(0) = m\Omega^2(Z_{cg} + r_h)c_\beta \begin{bmatrix} -s_\beta s_\theta \\ s_\beta c_\theta \\ c_\beta \end{bmatrix} \quad (30)$$

and

$$\mathbf{M}_{iner,1}(0) = \Omega^2(I_0 + Z_{cg}mr_h)c_\beta \begin{bmatrix} -s_\beta c_\theta \\ -s_\beta s_\theta \\ 0 \end{bmatrix} \quad (31)$$

where I_0 is the blade mass moment of inertia about its root and is given by

$$I_0 = \int_0^L m' z^2 dz \quad (32)$$

Rotor rotation causes a centrifugal traction force that is applied in the blade's longitudinal axis direction for a rotor without coning. As the coning angle increase, the out-of-plane component of this inertial force also increases generating loads that are in the same directions as the aerodynamic loads in normal operation. However, this phenomenon is reduced by the out-of-plane deflection of the blade.

Inertial loads due to rotor acceleration

This load component is given by the second term of Eq. 10. In the blade coordinate system, these loads are:

$$\mathbf{p}_{iner,2} = -m' \dot{\Omega} (z + r_h) c_\beta \begin{bmatrix} c_\theta \\ s_\theta \\ 0 \end{bmatrix} \quad (33)$$

and internal loads at blade root are:

$$\mathbf{V}_{iner,2}(0) = -m \dot{\Omega} (Z_{cg} + r_h) c_\beta \begin{bmatrix} c_\theta \\ s_\theta \\ 0 \end{bmatrix} \quad (34)$$

$$\mathbf{M}_{iner,2}(0) = -\dot{\Omega} (I_0 + Z_{cg} m r_h) c_\beta \begin{bmatrix} -s_\theta \\ c_\theta \\ 0 \end{bmatrix} \quad (35)$$

Rotor acceleration and deceleration create in-plane loads only. When the rotor is accelerating, the resulting inertial load is in the opposite direction of aerodynamic loads in normal operation. When braking, inertial loads add to aerodynamic loads. Tilt angle has no effect on these loads and a coning tend to slightly reduce them by a factor $\cos \beta$.

Inertial loads due to nacelle rotation

The third term of Eq. 10 gives the loads caused by the rotation of the wind turbine nacelle:

$$\mathbf{p}_{iner,3} = -m'(z) \Lambda^2 \begin{bmatrix} (z + r_h)(2c_\beta^2 c_\gamma s_\gamma c_\Psi s_\theta - c_\gamma s_\gamma c_\Psi s_\theta + c_\beta s_\beta s_\gamma^2 s_\theta \\ -c_\beta s_\beta c_\gamma^2 c_\Psi^2 s_\theta - s_\beta c_\gamma s_\gamma s_\Psi c_\theta - c_\beta c_\gamma^2 c_\Psi s_\Psi c_\theta) \\ + L_{nr}(-c_\beta c_\gamma^2 s_\theta - c_\gamma s_\gamma s_\Psi c_\theta - s_\beta c_\gamma s_\gamma c_\Psi s_\theta) \\ (z + r_h)(-2c_\beta^2 c_\gamma s_\gamma c_\Psi c_\theta + c_\beta s_\beta c_\gamma^2 c_\Psi^2 c_\theta - s_\beta c_\gamma s_\gamma s_\Psi s_\theta \\ -c_\beta c_\gamma^2 c_\Psi s_\Psi s_\theta - c_\beta s_\beta s_\gamma^2 c_\theta + c_\gamma s_\gamma c_\Psi c_\theta) \\ + L_{nr}(-c_\gamma s_\gamma s_\Psi s_\theta + s_\beta c_\gamma s_\gamma c_\Psi c_\theta + c_\beta c_\gamma^2 c_\theta) \\ (z + r_h)(+2c_\beta s_\beta c_\gamma s_\gamma c_\Psi + c_\beta^2 c_\gamma^2 c_\Psi^2 - c_\beta^2 s_\gamma^2 - c_\gamma^2) \\ + L_{nr}(+c_\beta c_\gamma s_\gamma c_\Psi - s_\beta c_\gamma^2) \end{bmatrix} \quad (36)$$

and the internal loads at blade root are:

$$\mathbf{V}_{iner,3} = -m\Lambda^2 \begin{bmatrix} (Z_{cg} + r_h)(2c_\beta^2 c_\gamma s_\gamma c_\Psi s_\theta - c_\gamma s_\gamma c_\Psi s_\theta + c_\beta s_\beta s_\gamma^2 s_\theta \\ -c_\beta s_\beta c_\gamma^2 c_\Psi^2 s_\theta - s_\beta c_\gamma s_\gamma s_\Psi c_\theta - c_\beta c_\gamma^2 c_\Psi s_\Psi c_\theta) \\ + L_{nr}(-c_\beta c_\gamma^2 s_\theta - c_\gamma s_\gamma s_\Psi c_\theta - s_\beta c_\gamma s_\gamma c_\Psi s_\theta) \\ (Z_{cg} + r_h)(-2c_\beta^2 c_\gamma s_\gamma c_\Psi c_\theta + c_\beta s_\beta c_\gamma^2 c_\Psi^2 c_\theta - s_\beta c_\gamma s_\gamma s_\Psi s_\theta \\ -c_\beta c_\gamma^2 c_\Psi s_\Psi s_\theta - c_\beta s_\beta s_\gamma^2 c_\theta + c_\gamma s_\gamma c_\Psi c_\theta) \\ + L_{nr}(-c_\gamma s_\gamma s_\Psi s_\theta + s_\beta c_\gamma s_\gamma c_\Psi c_\theta + c_\beta c_\gamma^2 c_\theta) \\ (Z_{cg} + r_h)(+2c_\beta s_\beta c_\gamma s_\gamma c_\Psi + c_\beta^2 c_\gamma^2 c_\Psi^2 - c_\beta^2 s_\gamma^2 - c_\gamma^2) \\ + L_{nr}(+c_\beta c_\gamma s_\gamma c_\Psi - s_\beta c_\gamma^2) \end{bmatrix} \quad (37)$$

$$\mathbf{M}_{iner,3} = -\Lambda^2 \begin{bmatrix} -(I_0 + mZ_{cg}r_h)(-2c_\beta^2 c_\gamma s_\gamma c_\Psi c_\theta + c_\beta s_\beta c_\gamma^2 c_\Psi^2 c_\theta - s_\beta c_\gamma s_\gamma s_\Psi s_\theta \\ -c_\beta c_\gamma^2 c_\Psi s_\Psi s_\theta - c_\beta s_\beta s_\gamma^2 c_\theta + c_\gamma s_\gamma c_\Psi c_\theta) \\ -mZ_{cg}L_{nr}(-c_\gamma s_\gamma s_\Psi s_\theta + s_\beta c_\gamma s_\gamma c_\Psi c_\theta + c_\beta c_\gamma^2 c_\theta) \\ (I_0 + mZ_{cg}r_h)(2c_\beta^2 c_\gamma s_\gamma c_\Psi s_\theta - c_\gamma s_\gamma c_\Psi s_\theta + c_\beta s_\beta s_\gamma^2 s_\theta \\ -c_\beta s_\beta c_\gamma^2 c_\Psi^2 s_\theta - s_\beta c_\gamma s_\gamma s_\Psi c_\theta - c_\beta c_\gamma^2 c_\Psi s_\Psi c_\theta) \\ +mZ_{cg}L_{nr}(-c_\beta c_\gamma^2 s_\theta - c_\gamma s_\gamma s_\Psi c_\theta - s_\beta c_\gamma s_\gamma c_\Psi s_\theta) \\ 0 \end{bmatrix} \quad (38)$$

For the sake of simplicity, the analysis of this load type is made for the particular case where the coning, tilt and pitch angle are zero ($\theta = \gamma = \beta = 0$). To distinguish with the complete solution, the variables are identified with a star (*) superscript symbol. In that case, the rotation and position vectors are

$$\mathbf{r}_{P/n}^* = \begin{bmatrix} 0 \\ -L_{nr} \\ z + r_h \end{bmatrix} \quad (39)$$

and

$$\mathbf{A}_n^* = \begin{bmatrix} -s_\Psi \\ 0 \\ c_\Psi \end{bmatrix} \quad (40)$$

The load distribution is then given by

$$\mathbf{P}_{iner,3}^* = m'\Lambda^2 \begin{bmatrix} (z + r_h)s_\Psi c_\Psi \\ -L_{nr} \\ (z + r_h)s_\Psi^2 \end{bmatrix} \quad (41)$$

and the internal loads at root are

$$\mathbf{V}_{iner,3}^*(0) = m\Lambda^2 \begin{bmatrix} (Z_{cg} + r_h)s_\Psi c_\Psi \\ -L_{nr} \\ (Z_{cg} + r_h)s_\Psi^2 \end{bmatrix} \quad (42)$$

$$\mathbf{M}_{iner,3}^*(0) = \Lambda^2 \begin{bmatrix} mZ_{cg}L_{nr} \\ (I_0 + mZ_{cg}r_h)s_\Psi c_\Psi \\ 0 \end{bmatrix} \quad (43)$$

Under these conditions, a rotation of the nacelle in any direction causes a constant negative flapwise loading and an edgewise loading that depends on the blade azimuth position. The latter is zero when the blade is in the horizontal and vertical position, reaches a maximum value at azimuth angles of 45° and 225° and a minimum value at azimuth angles of 135° and 315° . An axial force is also created by the nacelle rotation. This force is always null (when the blade is in the vertical position) or positive, reaching a maximum value when the blade is in the horizontal position.

Inertial loads due to nacelle acceleration

The fourth term of Eq. 10 gives the load caused by the acceleration of the wind turbine nacelle:

$$\mathbf{p}_{iner,4} = -m'(z)\dot{\Lambda} \begin{bmatrix} (z+r_h)(s_\beta c_\gamma c_\Psi c_\theta - c_\gamma s_\Psi s_\theta - c_\beta s_\gamma c_\theta) \\ + L_{nr}(c_\gamma c_\Psi c_\theta - s_\beta c_\gamma s_\Psi s_\theta) \\ (z+r_h)(s_\beta c_\gamma c_\Psi s_\theta - c_\beta s_\gamma s_\theta + c_\gamma s_\Psi c_\theta) \\ + L_{nr}(c_\gamma c_\Psi s_\theta + s_\beta c_\gamma s_\Psi c_\theta) \\ L_{nr}c_\beta c_\gamma s_\Psi \end{bmatrix} \quad (44)$$

and the internal loads at blade root are:

$$\mathbf{v}_{iner,4} = -m\dot{\Lambda} \begin{bmatrix} (Z_{cg}+r_h)(s_\beta c_\gamma c_\Psi c_\theta - c_\gamma s_\Psi s_\theta - c_\beta s_\gamma c_\theta) \\ + L_{nr}(c_\gamma c_\Psi c_\theta - s_\beta c_\gamma s_\Psi s_\theta) \\ (Z_{cg}+r_h)(s_\beta c_\gamma c_\Psi s_\theta - c_\beta s_\gamma s_\theta + c_\gamma s_\Psi c_\theta) \\ + L_{nr}(c_\gamma c_\Psi s_\theta + s_\beta c_\gamma s_\Psi c_\theta) \\ L_{nr}c_\beta c_\gamma s_\Psi \end{bmatrix} \quad (45)$$

$$\mathbf{M}_{iner,4} = -\dot{\Lambda} \begin{bmatrix} -(I_0 + mZ_{cg}r_h)(s_\beta c_\gamma c_\Psi s_\theta - c_\beta s_\gamma s_\theta + c_\gamma s_\Psi c_\theta) \\ -mZ_{cg}L_{nr}(c_\gamma c_\Psi s_\theta + s_\beta c_\gamma s_\Psi c_\theta) \\ (I_0 + mZ_{cg}r_h)(s_\beta c_\gamma c_\Psi c_\theta - c_\gamma s_\Psi s_\theta - c_\beta s_\gamma c_\theta) \\ +mZ_{cg}L_{nr}(c_\gamma c_\Psi c_\theta - s_\beta c_\gamma s_\Psi s_\theta) \\ 0 \end{bmatrix} \quad (46)$$

As for the previous case, an example will be given for a turbine with no coning and tilt and with a pitch angle of 0° . The position and rotation vectors are then the same as stated in the previous section and the load distribution on the blade is:

$$\mathbf{p}_{iner,4}^* = -m'\dot{\Lambda} \begin{bmatrix} L_{nr}c_\Psi \\ (z+r_h)s_\Psi \\ L_{nr}s_\Psi \end{bmatrix} \quad (47)$$

$$\mathbf{v}_{iner,4}^*(0) = -m\dot{\Lambda} \begin{bmatrix} L_{nr}c_\Psi \\ (Z_{cg}+r_h)s_\Psi \\ L_{nr}s_\Psi \end{bmatrix} \quad (48)$$

$$\mathbf{M}_{iner,4}^*(0) = -\dot{\Lambda} \begin{bmatrix} -(I_0 + mZ_{cg}r_h)s_\Psi \\ mZ_{cg}L_{nr}c_\Psi \\ 0 \end{bmatrix} \quad (49)$$

In the particular conditions stated above, the nacelle acceleration causes axial, in-plane and out-of-plane loads that depend on the direction of the acceleration. In-plane forces are zero when the blade is in the horizontal position and reach their extremum values when the blade is in the vertical position. The out-of-plane and axial forces are null when the blade is in the vertical position and reach their extremum values when the blade is in the horizontal position.

Inertial loads due to gyroscopic effect

The last inertial effect, given by the fifth term of Eq. 10 is the gyroscopic load due to the combination of rotor and nacelle rotations. The distribution of the load along blade length is given by:

$$\mathbf{p}_{iner,5} = -2m'\Lambda\Omega(z + r_h)c_\beta \begin{bmatrix} -(c_\beta c_\gamma c_\Psi + s_\beta s_\gamma)s_\theta \\ (c_\beta c_\gamma c_\Psi + s_\beta s_\gamma)c_\theta \\ -(s_\beta c_\gamma c_\Psi - c_\beta s_\gamma) \end{bmatrix} \quad (50)$$

and the forces and bending moments at blade roots are:

$$\mathbf{V}_{iner,5}(0) = -2m\Lambda\Omega(Z_{cg} + r_h)c_\beta \begin{bmatrix} -(c_\beta c_\gamma c_\Psi + s_\beta s_\gamma)s_\theta \\ (c_\beta c_\gamma c_\Psi + s_\beta s_\gamma)c_\theta \\ -(s_\beta c_\gamma c_\Psi - c_\beta s_\gamma) \end{bmatrix} \quad (51)$$

$$\mathbf{M}_{iner,5}(0) = 2\Lambda\Omega(I_0 + Z_{cg}mr_h)(c_\beta^2 c_\gamma c_\Psi + s_\beta c_\beta s_\gamma) \begin{bmatrix} c_\theta \\ s_\theta \\ 0 \end{bmatrix} \quad (52)$$

Assuming that the coning and tilt angles are small, gyroscopic effects cause loads that are mostly in the out-of-plane direction with extreme values reached when the blade is in the vertical position.

Application of loads in a three-dimensional finite element model

As discussed in the introduction, different methods can be used to transfer the loads computed by aeroelastic simulations to a finite element model. One of them is to apply the complete set of loads (including aerodynamic, gravitational and inertial loads) at the same time. These loads are often output as internal load distributions. A step of processing is then necessary to obtain the external load distribution that results in the given internal load distribution. Once the load distribution is known, the method of applying them to the finite element model is similar to that of aerodynamic loads presented in the next subsection.

The approach used in the following sections separates the different load types, applying the gravitational and inertial loads as volume loads.

Aerodynamic loads

The aerodynamic load on a wind turbine blade is a complex pressure and friction distribution. In some situations, knowing the angle of attack and the relative wind speed at a given location, it is possible to retrieve the pressure and friction distributions from airfoil data and apply them to the finite element model. However, in other situations, this distribution is not known. Airfoil data (lift, drag and moment

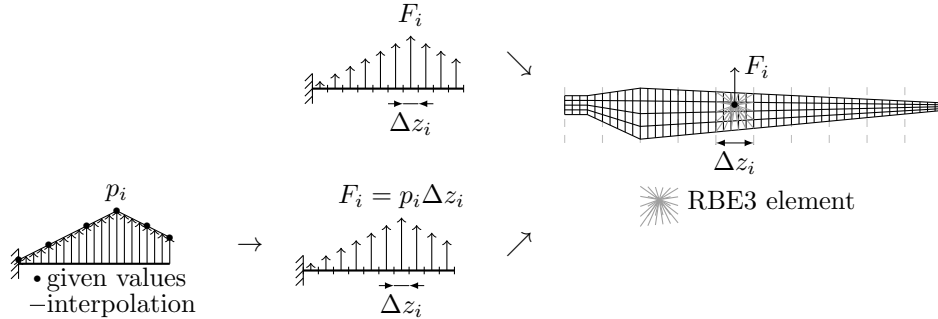


Figure 2. Method for the application of aerodynamic loads on a shell finite element model. F_i represents a concentrated force or moment and p_i , a force or moment per unit length.

coefficients from wind tunnel tests or numerical simulations) are often given only for a small range of angles of attack (approx. -5° to 15°). They are then extrapolated using empirical relations to cover the -180° to 180° range with no information about the pressure and friction distributions. There are also empirical corrections to BEM theory (hub and tip loss factors, Glauert correction for high values of induction factor, stall delay, dynamic stall, ...) that change aerodynamic lift, drag and moment with no information on the pressure and friction distribution modifications (Hansen 2008; Ning 2013).

For these reasons, it is difficult to reproduce the exact pressure and friction distributions over the blade surface. But an efficient approach to apply aerodynamic loads on a shell finite element model of a wind turbine blade does not have to do it. It is sufficient to assure that the internal force and moment distributions (beam loads) over the blade are correct, neglecting local load application effects that are not important for structural design purpose. The stress and strain fields at a given location depend mostly on the internal loads at that location (result of applied loads outboard of this location) and very little on the locally applied loads.

Aerodynamic loads could typically be given in two ways : (1) as concentrated forces and moments at the center of finite length aerodynamic elements or (2) as forces and moments per unit length given at some locations supposing linear interpolation between them. In both cases there are two forces (in-plane and out-of-plane) and a pitching moment (around the blade longitudinal axis). When loads are obtained as the second way, it could be transformed like the first way by dividing the blade in several sections, interpolating to get the load per unit length at the center of each section and multiplying by the length of each section to get the total load (see Fig. 2).

As seen in the introduction, different approaches exist for applying these loads on the shell finite element model. The preferred method is to use interpolation elements (Nastran's RBE3). This kind of element allow the loads applied to a reference node to be transferred on connected nodes with no stiffening of the structure. One interpolation element is created at each blade section or aerodynamic element. The reference node (the one where the forces and moments are applied) is located at the center of the section, on the blade's longitudinal axis. The connected nodes are all nodes covered by the blade section or aerodynamic element. Figure 2 shows the aerodynamic load application process.

Gravitational loads

In the finite element model, where the global coordinate system is the blade coordinate system, gravity induced loads can easily be accounted for by applying gravity in the \mathbf{g} direction. This direction is given by the unit vector (see Eq. 24):

$$\hat{\mathbf{g}} = \frac{\mathbf{g}}{g} = \begin{bmatrix} c_\gamma s_\Psi c_\theta - (c_\beta s_\gamma - s_\beta c_\gamma c_\Psi) s_\theta \\ c_\gamma s_\Psi s_\theta + (c_\beta s_\gamma - s_\beta c_\gamma c_\Psi) c_\theta \\ -s_\beta s_\gamma - c_\beta c_\gamma c_\Psi \end{bmatrix} \quad (53)$$

where $g = \|\mathbf{g}\| \approx 9.81 \text{ m/s}^2$.

Inertial loads due to rotor speed and acceleration

Finite element software packages allow the definition of this kind of volume load by defining an axis of rotation, a point through which this axis pass and rotation speed and acceleration. In this case, the axis of rotation is the positive y axis of the hub system:

$$\mathbf{A}_h = \begin{bmatrix} -c_\beta s_\theta \\ c_\beta c_\theta \\ -s_\beta \end{bmatrix} \quad (54)$$

and the point corresponding to the rotor center and through which the axis of rotation passes is

$$\mathbf{n}_h = \begin{bmatrix} 0 \\ 0 \\ -r_h \end{bmatrix} \quad (55)$$

When preparing the FE model, the user just has to define volume loads by specifying an angular speed Ω and acceleration $\dot{\Omega}$ around an axis defined by the unit vector \mathbf{A}_h and passing through point \mathbf{n}_h .

Inertial loads due to nacelle speed and acceleration

Here, (as for the centrifugal loads due to rotor speed and acceleration) an axis of rotation, a point through which this axis passes and a rotation speed and acceleration need to be defined. The axis of rotation is the positive z axis of the nacelle coordinate system. In the blade coordinate system, the rotation speed and acceleration vector is

$$\mathbf{A}_n = \begin{bmatrix} -(s_\beta c_\gamma c_\Psi - c_\beta s_\gamma) s_\theta - c_\gamma s_\Psi c_\theta \\ (s_\beta c_\gamma c_\Psi - c_\beta s_\gamma) c_\theta - c_\gamma s_\Psi s_\theta \\ c_\beta c_\gamma c_\Psi + s_\beta s_\gamma \end{bmatrix} \quad (56)$$

The point on the nacelle rotation axis is selected as the intersection point between the rotor axis and the nacelle rotation axis which is the origin of the nacelle coordinate system. In the blade coordinate system, this point is

$$\mathbf{n}_n = -L_{nr} \begin{bmatrix} s_\theta c_\beta \\ -c_\beta c_\theta \\ s_\beta + r_h/L_{nr} \end{bmatrix} \quad (57)$$

As for the previous case, when preparing the FE model, volume loads have to be defined by specifying an angular speed Λ and acceleration $\dot{\Lambda}$ around an axis defined by the unit vector \mathbf{A}_n and passing through point \mathbf{n}_n .

Inertial loads due to gyroscopic effects

The gyroscopic loads are harder to apply in a finite element model as most solvers have no methods implemented for that purpose. Making the assumption that all the blade mass is concentrated on its longitudinal axis and neglecting the axial loads (that are small compared to the in-plane and out-of-plane loads, especially if coning and tilt angles are small), it is possible to make an analogy between gyroscopic forces and forces due to an angular acceleration. Taking an angular acceleration of magnitude

$$\alpha_g = -2\Lambda\Omega c_\beta(c_\beta c_\gamma c_\Psi - s_\beta s_\gamma) \quad (58)$$

around the unit vector

$$\mathbf{A}_g = \begin{bmatrix} c_\theta \\ s_\theta \\ 0 \end{bmatrix} \quad (59)$$

and passing through the intersection point between the blade's longitudinal axis and the rotor axis

$$\mathbf{n}_h = \begin{bmatrix} 0 \\ 0 \\ -r_h \end{bmatrix} \quad (60)$$

This results in a force distribution equal to

$$\mathbf{p} = m' \alpha_g \mathbf{A}_g \times \left(\begin{bmatrix} 0 \\ 0 \\ z \end{bmatrix} - \mathbf{n}_h \right) = -2m' \Lambda \Omega c_\beta (c_\beta c_\gamma c_\Psi + s_\beta s_\gamma) (z + r_h) \begin{bmatrix} -s_\theta \\ c_\theta \\ 0 \end{bmatrix} \quad (61)$$

which is the same as Eq. 50 except that the axial component is neglected. This gives a practical way to include gyroscopic loads in the finite element model even if this kind of load is not implemented in the solver used. The resulting applied load distribution will be close to the real distribution if the coning and tilt angles are small and if the blade mass is concentrated close to its longitudinal axis.

Application on the WESNet 10 kW wind turbine

To illustrate the method described above, one of the critical load cases of the WESNet 10 kW wind turbine (Forcier et al. 2013) is studied. This turbine, with its downwind free yaw configuration and its variable speed rotor, offers a good example as all the load components discussed in this paper are likely to occur. The turbine and blade characteristics that are necessary to compute the loads are as follows: $m = 28.00$ kg, $Z_{cg} = 0.9100$ m, $I_0 = 47.66$ kg·m², $L_{nr} = -0.63$ m, $r_h = 0.28$ m, $\beta = -3^\circ$, $\gamma = 0^\circ$. Note that since the rotor has a downwind configuration with a downwind coning, the overhang length and coning angle have negative values.

The studied load case was obtained from a simulation using the NREL's FAST aeroelastic software (Jonkman and Buhl Jr. 2005). To conform to the hypotheses of this paper, the blade, tower and shaft deformation degrees of freedom were disabled during the FAST simulation. This software supposes, as in this paper, that the blade mass is concentrated on its longitudinal axis.

The example load case arises during an extreme operating gust (IEC 61400-2 design load case 1.3 at rated wind speed of 9.5 m/s). The gust causes an acceleration of the rotor, which causes yawing of

Table 1. Load case used in the numerical application. z and Δz are respectively the blade's aerodynamic element center and length. F_T and F_N are respectively the tangential and normal aerodynamic forces on the element. F_T is in the x direction of the cone coordinate system of this paper and F_N is in the y direction of this same coordinate system. M_P is the pitching moment, positive when leading edge goes downwind (around z axis of the blade or cone coordinate system of this paper).

z [m]	Δz [m]	F_T [N]	F_N [N]	M_P [N·m]
0.1034	0.207	0.000	0.000	0.243
0.3334	0.253	0.000	0.000	1.097
0.5600	0.200	31.160	13.133	-0.744
0.7600	0.200	40.094	15.693	-0.812
0.9600	0.200	34.318	12.698	-1.126
1.1600	0.200	37.074	12.307	-1.085
1.3600	0.200	41.319	13.582	-0.289
1.5600	0.200	49.033	15.036	0.031
1.7600	0.200	51.525	13.360	-0.275
1.9600	0.200	45.504	9.104	-0.270
2.1600	0.200	38.053	5.495	-0.517
2.3600	0.200	22.920	2.056	-0.601
2.5600	0.200	19.079	0.812	-0.638
2.8100	0.300	12.848	-0.688	-1.116
3.0600	0.200	-0.345	-0.875	-0.768
3.2600	0.200	-5.879	-0.752	-0.730
3.4600	0.200	-7.169	-0.534	-0.639
3.6600	0.200	-0.067	-0.794	-0.495

$\theta = -2.021^\circ = -0.03527$ rad
 $\Psi = 183.9^\circ = 3.210$ rad
 $\Omega = 222.1$ rpm = 23.26 rad/s
 $\dot{\Omega} = 65.47^\circ/\text{s}^2 = 1.143$ rad/s²
 $\Lambda = -71.22^\circ/\text{s} = -1.243$ rad/s
 $\dot{\Lambda} = -234.9^\circ/\text{s}^2 = -4.100$ rad/s²
 $g = 9.81$ m/s²

the free yaw nacelle. The result is a combination of inertial loads due to rotor speed and acceleration; nacelle speed and acceleration; and gyroscopic effect due to rotor and nacelle rotation. Table 1 presents the aerodynamic loads and wind turbine operation parameters for this particular load case.

Taking the information of Table 1 and the mass, inertia and turbine configuration data presented above, Eq. 21, 22, 25, 26, 30, 31, 34, 35, 37, 38, 45, 46, 51 and 52 can be used to compute loads of all types. These results are presented in Table 2 ("This work" column). Also presented in this table are the internal forces and moments at root given by the aeroelastic model. Only total loads are presented as FAST does not output separated load types. A shell finite element model of the blade has been made and loads have been applied as presented in the section beginning at page 14. The Altair's Optistruct finite element solver was used to evaluate all load types separately and then, all together and the total applied loads were output and presented in Table 2 ("FEM" column). For a description of the FE model, see Forcier et al. (2013).

Reminding that the critical load component is frequently the flapwise bending moment, we will now focus our attention on it. According to the blade coordinate system used here, this bending moment is M_x

Table 2. Internal forces and moments at blade root. Forces are in N and moments, in N-m. Column "This work" computed from the equations of section starting on page 8. For the "FAST" column, loads are converted from FAST blade coordinate system to this work coordinate system: $V_x = -\text{RootFybl}$, $V_y = \text{RootFxb1}$, $N = \text{RootFzbl}$, $M_x = -\text{RootMybl}$, $M_y = \text{RootMxb1}$, $M_t = \text{RootMzc1}$.

Load	This work	FAST	Detailed	FEM	Diff. 1	Diff. 2	Diff. 3
$V_{x,aero}$	124.0	-	124.0	124.0	-	0.00	0.00
$V_{y,aero}$	405.3	-	405.3	405.3	-	0.01	0.01
N_{aero}	0.000	-	0.000	0	-	-	-
$M_{x,aero}$	-607.2	-	-607.2	-607.2	-	0.00	0.00
$M_{y,aero}$	157.5	-	157.5	157.5	-	0.02	0.02
$M_{t,aero}$	-8.734	-	-8.734	-8.734	-	0.00	0.00
$V_{x,grav}$	-19.18	-	-19.18	-19.18	-	-0.02	-0.03
$V_{y,grav}$	-13.68	-	-13.67	-13.67	-	0.04	0.03
N_{grav}	273.7	-	273.7	273.6	-	0.02	0.02
$M_{x,grav}$	12.44	-	13.87	13.87	-	-10.28	-0.01
$M_{y,grav}$	-17.45	-	-12.34	-12.34	-	41.42	-0.04
$M_{t,grav}$	0.000	-	0.3555	0.3549	-	-100.00	0.03
$V_{x,iner,1}$	-33.22	-	-319.0	-318.6	-	-89.57	0.13
$V_{y,iner,1}$	-941.4	-	-931.3	-931.4	-	1.08	-0.01
$N_{iner,1}$	17970	-	17970	17980	-	-0.03	-0.03
$M_{x,iner,1}$	1548	-	1645	1644	-	-5.83	0.05
$M_{y,iner,1}$	-54.63	-	20.39	20.29	-	-369.26	0.48
$M_{t,iner,1}$	0.000	-	32.32	32.27	-	-100.00	0.17
$V_{x,iner,2}$	-38.00	-	-38.00	-38.00	-	-0.01	-0.01
$V_{y,iner,2}$	1.341	-	1.372	1.372	-	-2.26	0.00
$N_{iner,2}$	0.000	-	-0.6032	-0.6023	-	-100.00	0.12
$M_{x,iner,2}$	-2.205	-	-2.267	-2.268	-	-2.78	-0.04
$M_{y,iner,2}$	-62.49	-	-62.56	-62.58	-	-0.15	-0.03
$M_{t,iner,2}$	0.000	-	0.1946	0.1928	-	-100.00	1.14
$V_{x,iner,3}$	4.541	-	3.735	3.737	-	21.51	-0.05
$V_{y,iner,3}$	29.76	-	29.98	29.98	-	-0.75	0.00
$N_{iner,3}$	1.805	-	1.760	1.760	-	2.56	0.00
$M_{x,iner,3}$	-28.95	-	-29.20	-29.20	-	-0.85	0.01
$M_{y,iner,3}$	6.762	-	5.863	5.865	-	15.29	-0.03
$M_{t,iner,3}$	0.000	-	-0.5934	-0.5925	-	-100.00	0.08
$V_{x,iner,4}$	78.90	-	79.49	79.49	-	-0.74	0.00
$V_{y,iner,4}$	-12.34	-	-10.20	-10.20	-	20.97	0.01
$N_{iner,4}$	4.912	-	5.060	5.060	-	-2.92	0.00
$M_{x,iner,4}$	18.23	-	15.85	15.86	-	14.96	-0.09
$M_{y,iner,4}$	76.79	-	77.61	77.62	-	-1.07	-0.01
$M_{t,iner,4}$	0.000	-	-1.107	-1.201	-	-100.00	-7.83
$V_{x,iner,5}$	-67.60	-	-67.67	-67.62	-	-0.03	0.08
$V_{y,iner,5}$	-1916	-	-1918	-1916	-	-0.02	0.09
$N_{iner,5}$	-100.5	-	-100.6	7.290	-	-1478.04	-1479.51
$M_{x,iner,5}$	3150	-	3147	3151	-	-0.02	-0.13
$M_{y,iner,5}$	-111.2	-	-113.3	-110.0	-	1.06	3.02
$M_{t,iner,5}$	0.000	-	43.42	42.77	-	-100.00	1.53
$V_{x,total}$	49.45	49.47	-236.6	-236.1	-0.04	-120.94	0.22
$V_{y,total}$	-2447	-2446	-2436	-2435	0.03	0.48	0.05
N_{total}	18150	18150	18150	18260	0.03	-0.58	-0.58
$M_{x,total}$	4091	4091	4183	4186	0.00	-2.27	-0.08
$M_{y,total}$	-4.653	-4.626	73.17	76.39	0.58	-106.09	-4.21
$M_{t,total}$	-8.734	-8.733	65.86	65.06	0.01	-113.42	1.24

Diff. 1: (This work-FAST)/(FAST) × 100

Diff. 2: (This work-FEM)/(FEM) × 100

Diff. 3: (Detailed-FEM)/(FEM) × 100

and should be negative in normal operation (i.e., when aerodynamic loads are dominant; see Figure 1). However, one of the critical load cases resulting from the analysis of the WESNet wind turbine (the one studied in this section) yields a flapwise bending moment that is in the opposite direction (positive value of M_x). The equations developed in section starting on page 8 are useful to understand this load case.

First, we can observe that the aerodynamic flapwise bending moment is effectively in the normal direction. The dominant load types in this load case are the inertial loads due to rotor rotation ($M_{x,iner,1}$) and to the gyroscopic effects due to a combination of rotor and nacelle rotations ($M_{x,iner,5}$), the latter being the most important. This analysis gives insight about some solutions to reduce the loads associated with this load case. The installation of a damping system to reduce the nacelle rotation speed would reduce the gyroscopic loads. Another solution could be to limit the rotation speed of the rotor. Finally, looking at Equation 31, we can conclude that a reduction of the coning angle would reduce the flapwise bending moment due to rotor rotation. Nevertheless we have to take into account that the blade is not perfectly rigid so that the blade will deform and this could slightly change the conclusion drawn from an analysis with rigid blades.

When comparing the total load values of this work with values output by the FAST aeroelastic solver (Table 2), all differences are within a margin of 0.05 % except for the difference in M_y value. This is probably caused by a rounding error of the azimuth angle (for that angle, sine computation amplifies the error). However, when comparing the root load values obtained from the equations of section starting on page 8 with the summed loads at root in the finite element model, some load types and directions show an important difference. This is due to the fact that, in the finite element model, blade mass is not concentrated on its longitudinal axis. The values obtained from the finite element model are more precise because they take into account the real mass distribution of the blade. This causes loads on blade that are slightly different than what is predicted by the equations of section starting on page 8 and by an aeroelastic solver that suppose that blade mass is concentrated on its longitudinal axis. These differences are noticed in the edgewise loads and torsional moment. On the other hand, the error in flapwise loads and axial force (that are the critical loads) is minimal.

To get the same values as those obtained in the finite element model, it is possible to recompute the equations of section starting on page 8 by using a different form of Equation 10 where the blade mass is not supposed to be concentrated on its longitudinal axis:

$$\begin{aligned}
 \mathbf{f}_{iner} = & -\rho\boldsymbol{\omega}_{h/t} \times \boldsymbol{\omega}_{h/t} \times \mathbf{r}_{P/h} \\
 & -\rho\boldsymbol{\alpha}_{h/t} \times \mathbf{r}_{P/h} \\
 & -\rho\boldsymbol{\omega}_{n/T} \times \boldsymbol{\omega}_{n/T} \times \mathbf{r}_{P/n} \\
 & -\rho\boldsymbol{\alpha}_{n/T} \times \mathbf{r}_{P/n} \\
 & -2\rho\boldsymbol{\omega}_{n/T} \times \boldsymbol{\omega}_{h/t} \times \mathbf{r}_{P/h}
 \end{aligned} \tag{62}$$

where ρ is the material density and \mathbf{f}_{iner} is the inertial force per unit volume at a given infinitesimal point on the blade. When using the position vector $\mathbf{r}_{P/b} = [x, y, z]^T$ instead of $\mathbf{r}_{P/b} = [0, 0, z]^T$ and integrating over the surface of each cross section, the distribution of force and moment per unit length of the blade can be expressed in function of each cross section's mass per unit length (m'), center of gravity (x_{cg} and y_{cg}) and mass moment of inertia per unit length (i_x , i_y and i_{xy}). After that, integration over blade length gives internal loads at root that are functions of blade's mass (m), center of gravity (X_{cg} , Y_{cg} and Z_{cg}) and mass moment of inertia (I_x , I_y , I_z , I_{xy} , I_{xz} and I_{yz}).

Blade root internal loads computed this way for the example wind turbine are reported in table 2 ("Detailed" column) and show really small differences when compared to the finite element model values. The only noticeable difference is for the axial load caused by the gyroscopic effect ($N_{x,iner,5}$) but that difference is normal since the axial force is not taken into account by the method of applying this type of load in the finite element model as explained earlier. This confirms that the differences observed between values computed using equations of section starting on page 8 and the finite element model values are due to the different blade mass distribution in both models. One of the advantages of the proposed method is that the inertial loads are applied correctly using the real mass distribution of the blade.

Conclusion

One of the objectives of this paper was to propose a method to study the contributions of different load types in the total load on a wind turbine blade computed during an aeroelastic simulation. This has been done by developing analytical equations allowing the computation of the values of the different load types as a function of the wind turbine operation parameters (speed and acceleration of the rotor and the nacelle; azimuth and pitch angles), geometry (tilt and coning angle; rotor hub radius; distance between the tower axis and the rotor plane) and blade mass parameters. This set of equations could also be useful to determine the effects of some geometric and operation parameters on the wind turbine blade loads, especially at the preliminary stages of the design process.

The second objective was to describe a method to take the loads computed by an aeroelastic simulation and apply them to a three-dimensional finite element model of a blade. The proposed method consists in applying the aerodynamic loads using RBE3 elements and applying gravitational and inertial loads as volume forces. All the axes and points of rotation and acceleration are defined in order to apply the different inertial load types.

The advantages of this method are:

- The applied inertial loads take into account the real blade mass distribution around its longitudinal axis (with an exception for the gyroscopic load).
- A modification of the blade design that results in a change of its mass properties is directly accounted for in the applied loads of the finite element model. This is particularly useful for a finite element model using structural optimization: inertial and gravitational loads are automatically adjusted according to the blade mass properties during the optimization process.
- It is possible to apply a different safety factor on different load types if the standard used prescribes it.
- It is possible to study the effects of the wind turbine's geometric characteristics and operating conditions without the necessity of simulating a particular situation in an aeroelastic simulation.

All the methods and equations proposed in this paper are based on the hypothesis that the blade and the tower are rigid. Consequently, they are well designed for use in the preliminary stages of the design process, if the tower and the blades are considered rigid in the aeroelastic simulation. This allows the designer to get a first set of loads to start the design with minimal information about the blade mass.

However, even when modeling the blade and tower flexibility, the proposed equations could yield useful information for the understanding of the effects of the different load types on the total blade load.

References

- Bazilevs Y, Hsu MC, Akkerman I, Wright S, Takizawa K, Henicke B, Spielman T and Tezduyar TE (2011a) 3D simulation of wind turbine rotors at full scale. Part I: Geometry modeling and aerodynamics. *International Journal for Numerical Methods in Fluids* 65(1-3): 207–235.
- Bazilevs Y, Hsu MC, Kiendl J, Wüchner R and Bletzinger KU (2011b) 3D simulation of wind turbine rotors at full scale. Part II: Fluid–structure interaction modeling with composite blades. *International Journal for Numerical Methods in Fluids* 65(1-3): 236–253.
- Bir G (2005) User’s guide to PreComp (pre-processor for computing composite blade properties). Technical report, National Renewable Energy Laboratory, Golden (Colorado, United States).
- Blasques JP (2012) User’s manual for BECAS : A cross section analysis tool for anisotropic and inhomogeneous beam sections of arbitrary geometry. Technical Report Risø-R-1785(EN), Risø DTU – National Laboratory for Sustainable Energy, Roskilde (Denmark).
- Bossanyi EA (2003) GH Bladed theory manual. Technical Report 282/BR/009 issue 11, Garrad Hassan and Partners Limited.
- Caous D, Lavauzelle N, Valette J and Wahl JC (2018) Load application method for shell finite element model of wind turbine blade. *Wind Engineering*, Preprint.
- Chen H, Yu W and Capellaro M (2010) A critical assessment of computer tools for calculating composite wind turbine blade properties. *Wind Energy* 13(6): 497–516.
- Forcier LC, Sumner J, Gagnon T, Charron JF and Joncas S (2013) Structural design and validation of a 10 kW wind turbine blade. In: *19th International Conference on Composite Materials*. Montreal (Quebec, Canada), 28 July – 2 August.
- Griffith DT and Ashwill TD (2011) The Sandia 100-meter all-glass baseline wind turbine blade: SNL100-00. Technical Report SAND2011-3779, Sandia National Laboratories, Albuquerque (New Mexico, United States).
- Hansen MOL (2008) *Aerodynamics of Wind Turbines*. 2nd edition. London (United Kingdom): Earthscan.
- Jonkman JM (2003) Modeling of the UAE wind turbine for refinement of FAST_AD. Technical Report NREL/TP-500-34755, National Renewable Energy Laboratory, Golden (Colorado, United States).
- Jonkman JM and Buhl Jr ML (2005) FAST user’s guide. Technical Report NREL/EL-500-29798, National Renewable Energy Laboratory, Golden (Colorado, United States).
- Knill TJ (2005) The application of aeroelastic analysis output load distributions to finite element models of wind. *Wind Engineering* 29(2): 153–168.
- Knowledge Centre WMC (2012) FOCUS6: The integrated wind turbine design suite. Knowledge Centre WMC, Wieringerwerf (The Netherlands).
- Larsen TJ and Hansen AM (2007) How 2 HAWC2, the user’s manual. Technical Report Risø-R-1597(ver. 3-1)(EN), Risø National Laboratory, Roskilde (Denmark).
- Lillo P (2011) Static and fatigue analysis of wind turbine blades subject to cold weather conditions using finite element analysis, Master’s thesis, University of Victoria, Victoria (British Columbia, Canada).
- Lindenburg C (2005) PHATAS release "NOV-2003" and "APR-2005" user’s manual. Technical Report ECN-I--05-005, Energy Research Center of the Netherlands, Petten (The Netherlands).
- Lindenburg C and de Winkel GD (2005a) Buckling load prediction tools for rotor blades. Mode description of tools for buckling of thin-walled beams. Technical Report ECN-C--05-103, Energy Research Center of the Netherlands, Petten (The Netherlands).

- Lindenburg C and de Winkel GD (2005b) State of the art of rotor blade buckling tools: Inventory of the Dutch BLADKNIK project. Technical Report ECN-C--05-054, Energy Research Center of the Netherlands, Petten (The Netherlands).
- Malcolm DJ and Laird DL (2007) Extraction of equivalent beam properties from blade models. *Wind Energy* 10: 135–157.
- Ning S (2013) AirfoilPrep.py documentation. Technical Report NREL/TP-5000-58817, National Renewable Energy Laboratory, Golden (Colorado, United States).
- Wang Q, Sprague MA, Jonkman J, Johnson N and Jonkman B (2017) BeamDyn: a high-fidelity wind turbine blade solver in the FAST modular framework. *Wind Energy* 20(8): 1439–1462.
- Wilson RE, Walker SN and Heh P (1999) Technical and user's manual for the FAST_AD advanced dynamics code. Technical Report OSU/NREL report 99-01, Oregon State University and National Renewable Energy Laboratory, Corvallis (Oregon, United States) and Golden (Colorado, United States).
- Yu W, Hodges DH, Volovoi V and Cesnik CE (2002) On Timoshenko-like modeling of initially curved and twisted composite beams. *International Journal of Solids and Structures* 39(19): 5101–5121.